Received: 15 May 2023 | Revised: 25 August 2023 | Accepted: 1 September 2023

DOI: 10.1002/jbm.a.37614

RESEARCH ARTICLE

Society For Biomaterials | WILEY

Heparin–collagen I bilayers stimulate FAK/ERK½ signaling via α2β1 integrin to support the growth and anti-inflammatory potency of mesenchymal stromal cells

Said J. Cifuentes[1] | Maribella Domenech[1,2]

[1]Bioengineering Graduate Program, University of Puerto Rico Mayaguez, Mayaguez, Puerto Rico, USA

[2]Department of Chemical Engineering, University of Puerto Rico Mayaguez, Mayaguez, Puerto Rico, USA

Correspondence
Maribella Domenech, Bioengineering Graduate Program, University of Puerto Rico Mayaguez, Call Box 9000, Mayaguez, PR 00681-9000, USA.
Email: maribella.domenech@upr.edu

Funding information
Engineering Research Centers, Grant/Award Number: EEC-1648035

Abstract

Understanding mesenchymal stromal cells (MSCs) growth mechanisms in response to surface chemistries is essential to optimize culture methods for high-quality and robust cell yields in cell manufacturing applications. Heparin (HEP) and collagen 1 (COL) substrates have been reported to enhance cell adhesion, growth, viability, and secretory potential in MSCs. However, the biomolecular mechanisms underlying the benefits of combined HEP/COL substrates are unknown. This work used HEP/COL bilayered surfaces to investigate the role of integrin-HEP interactions in the advantages of MSC culture. The layer-by-layer approach (LbL) was used to create HEP/COL bilayers, which were made up of stacks of 8 and 9 layers that combined HEP and COL in an alternate arrangement. Surface spectroscopic investigations and laser scanning microscopy evaluations verified the biochemical fingerprint of each component and a total stacked bilayer thickness of roughly 150 nm. Cell growth and apoptosis in response to IC_{50} and IC_{75} levels of BTT-3033 and Cilengitide, α2β1 and αvβ3 integrin inhibitors respectively, were evaluated on HEP/COL coated surfaces using two bone marrow-derived MSC donors. While integrin activity did not affect cell growth rates, it significantly affected cell adhesion and apoptosis on HEP/COL surfaces. HEP-ending HEP/COL surfaces significantly increased FAK-ERK½ phosphorylation and endogenous cell COL deposition compared to COL, COL-ending HEP/COL and uncoated surfaces. BTT-3033 but not Cilengitide treatment markedly affected FAK-ERK½ activity levels on HEP-ending HEP/COL surfaces supporting a major role for α2β1 activity. BTT-3033 treatment on HEP-ending bilayers reduced MSC-mediated macrophage inhibitory activity and altered the cytokine profile of co-cultures. Overall, this study supports a novel role for HEP in regulating the survival and potency of MSCs via enhancing the α2β1-FAK-ERK½ signaling mechanism.

KEYWORDS
collagen 1, heparin, human mesenchymal stromal cells, integrins, layer-by-layer

1 | INTRODUCTION

Over the past 30 years, the use of MSCs as cell therapies has attracted much attention due to their therapeutic value for tissue engineering applications and inflammatory conditions.[1] MSCs distinguish themselves from other cells by their innate differentiation potential and their plethora of secreted growth factors and cytokines of therapeutic value.[2] Altogether, these characteristics have fueled

more than 367 interventional clinical trials worldwide over the past two decades (https://clinicaltrials.gov/ct2/results?type=Intr&cond=MSC), demonstrating the immense potential of MSCs in medical research and the significant effort of exploring the use of MSCs from various tissues for the treatment of diverse diseases.

While multiple clinical applications of MSCs in regenerative medicine are being pursued, several manufacturing challenges limit their fast progress towards their clinical translation, including their dependence on biologics and increased replicative senescence during culture, limiting the achievements of high cell yields and their secretory potency.[3] Classical standard methods consist of several MSC expansion cycles, mainly on two-dimensional plastic surfaces, which are used for cell propagation but struggle to reach the billions count.[4] One main limitation of these standard culture surfaces is that they gradually lead to cell senescence and spontaneous differentiation while reducing the therapeutic potency of secreted factors from undifferentiated MSCs.[5] Altogether, these substrate-driven cell alterations significantly affect the therapeutic cell dosage and activity in-vivo.[6]

Alternative culture methods, such as the use of synthetic functionalized polymers, have been examined with encouraging results in the overall quality of cells. Examples include the RGD-modified alginate hydrogels reported by Ho et al.,[7] in which MSC-spheroids entrapped in hydrogels performed better than controls for cell survival, secreted factors, and bone formation. However, the absence of data supporting cell growth suggests that this platform is not optimal for cell propagation. Similarly, another study by Ogle et al.,[8] showed that regulation of substrate stiffness via RGD-functionalized PEG-DA hydrogels favored the potency of MSCs via the secretion of immunomodulatory factors but at a lower proliferative potential. Thus, the lack of strategies that prolong the longevity and quality of MSC limits their use in clinical applications.

In spite of recent progress, robust culture strategies that support high viability and cell yields of undifferentiated MSC still need to be met. This situation limits total cell yields due to the early termination of MSC cultures at low passages.[9] In addition, other events influence total cell yields, including low cell recovery rates due to cell detachments, early cell death, and an increase in replicative senescence often observed after prolonged cell contact with pristine tissue culture-treated plastic surfaces. One strategy to improve MSC stability and viability in culture is to employ integrin-binding culture surfaces. Current culture methods for MSC propagation display limited integrin cues relevant to MSC maintenance in tissues. For example, integrin and growth factor signaling are critical for maintaining MSC's quality attributes and monitoring their performance under physiologically relevant conditions.[10] While exogenous growth factors can be added in-vitro at a higher expense in cultures, stimulation of integrin signals is often overlooked in bioengineered culture substrates. Integrins are naturally stimulated in the native tissue, playing crucial roles in regulating cell differentiation,[11] proliferation/death,[12–14] cytoskeleton reorganization,[15] and migration.[16] Bare plastic surfaces cannot effectively stimulate integrins, while synthetic substrates that deliver RGD conjugates have limited integrin stimulatory activity. Culture substrates composed of full-length ECM components more effectively stimulate integrins than tissue culture plastics (TCP) and synthetic polymer conjugates due to the broad display of integrin motifs that support cell adhesion and viability.[17] Prior work from our group showed that culture substrates composed of COL nanofibers[18] best-supported tumor cell growth relative to gels and primitive COL forms under hormone-restrictive culture conditions. This enhanced cell growth process was mediated by $\alpha 2\beta 1$ integrin stimulation. Similarly, the importance of COL integrins has been highlighted in several studies, where collagen-integrin activity has been shown to promote cell survival and reduce apoptosis in hepatic stellate cells via $\alpha 2\beta 1$ integrin activation.[19] Additionally, $\alpha 2\beta 1$ and $\alpha 11\beta 1$ collagen-recognizing integrin receptors, but not $\alpha 1\beta 1$, were shown to promote MSC survival through Akt activation,[20] while disturbance of these interactions resulted in MSC cell death.

While the significance of COL integrins in regulating MSC behavior is widely recognized, their specific role in regulating the growth and potency of undifferentiated MSC is less understood, particularly within the context of cell manufacturing applications. Our group[21] and others[22,23] have shown that surfaces coated with substrates containing COL are beneficial for cell culture. In particular, utilizing multilayered substrates-composed of at least nine consecutive layers (9-L) of HEP and COL - instead of the individual components alone produces better outcomes. Our previous work[21] employed surface plasmon resonance (SPR) and ellipsometry analysis for characterizing HEP/COL multilayers. These analyses confirmed the continuous deposition of constituent materials, culminating with a HEP-ended coating of a thickness of approximately 100 nm. HEP-ended HEP/COL bilayers more effectively supported the expansion of MSCs and neural cells, thereby enhancing multiple facets of cell quality, including adhesion, growth, secretion, senescence, and responsiveness to trophic factors. Notably, attempting cell growth on single-coated HEP surfaces proved futile due to the high negative surface charge density and sulfate pattern that prevent cell adhesion, underscoring the intricate interplay between COL and HEP within cell culture. In dual-component sandwiched bilayers, COL provides anchoring motifs for cell adhesion via integrins while decreasing the total net surface charge,[24] and HEP allows the preservation of exogenously added and endogenous cell-secreted factors, enriching the local culture microenvironment.[25] Other studies indicate that HEP can promote not only augmented COL expression by MSCs,[26] but also enhanced integrin function in platelet aggregation, suggesting that HEP can contribute to enriched integrin activity.[27,28] In this study, we investigated the role of integrin activity in the anti-inflammatory potency and growth of undifferentiated MSCs on surface-deposited HEP/COL bilayers. A better understanding of HEP-integrin cross talk represents a novel opportunity for developing cell-instructive culture strategies supportive of high cell quality and yields for cell manufacturing applications.

2 | MATERIALS AND METHODS

2.1 | Surface deposition of HEP/COL multilayers

Lyophilized collagen 1 derived from bovine tendon from Integra Lifesciences Holdings Corporation (Añasco, PR) and heparin sodium (PH3005, Celsus Laboratories) solutions were prepared according to

the procedure previously described by Castilla-Casadiego et al.[29] Briefly, acetate buffer was prepared from 0.1 M sodium acetate anhydrous and 0.1 M acetic acid glacial in ultrapure 18 MΩ-cm water purified by Barnstead™ MicroPure™ Water Purification System (50132370, Thermo Fisher). HEP and COL were separately dissolved in acetate buffers at a concentration of 1.0 mg/mL. Stacked bilayers of HEP/COL were generated by the LbL surface coating method on TCP plates as described by us previously.[21] Briefly, surfaces are positively charged by a 15 min pre-incubation with 1.0 mg/mL polyethyleneimine (PEI) (P3143, Sigma-Aldrich) dissolved in acetate buffer. Each COL and HEP layer deposition consisted of 5 min incubation followed by a 3 min washing with acetate buffer. This procedure was repeated, alternating between HEP and COL solutions for up to nine total layers, ending with HEP as the outer layer. A final wash was performed using sterile Dulbecco's phosphate-buffered solution (DPBS) (D5652-10X1L, Sigma-Aldrich), and substrates were immediately sterilized inside the biosafety cabinet using UV light for 10 min.

2.2 | Multilayers characterization

HEP/COL multilayers were deposited onto silicon substrates as described in the previous section. The deposition process involved the automated dipping machine nanoStrata StratoSequence VI, which facilitated the sequential immersion of silicon substrates in each polymeric solution until the desired number of layers was achieved. Subsequently, the modified silicon substrates underwent infrared analysis (IR-VASE®-Mark II, J.A. Woollam) to confirm the chemical fingerprint of individual components on HEP/COL multilayers. Functional group identification was conducted within a wavenumber range spanning 800–1700 cm^{-1}. Measurements were acquired using a deuterated triglycine sulfate (DTGS) detector with an angle of incidence set at 70°. The spectral resolution was maintained at 16 cm^{-1}, with 200 scans performed in a single cycle. Additionally, rotating compensatory ellipsometry (RCE) analysis employed a bandwidth of 0, a minimum intensity ratio of 5, and incorporated a zone average polarizer and a rotating compensator analyzer set to zone average. Surfaces were characterized via non-invasive 3D laser scanning to estimate the multilayer thickness and surface roughness (VK-X1000, KEYENCE). An average of 140 images per sample were obtained to map the uncoated and coated regions at a magnification of 50X, superfine resolution, high precision quality, and a pitch of 0.1 μm. Next, the images were stitched together and analyzed using the KEYENCE VK Analyzer software to generate 3D surface profile data, encompassing roughness and thickness measurements.

2.3 | Mesenchymal stromal cell cultures

Bone marrow-derived stromal cells (BMSCs) from two donors (MSC-003, lot 00182, and lot 310271) were purchased from RoosterBio®. Based on the cell product specification data sheets provided by the company, these cells were positive for CD90 and CD166 and negative for CD34 and CD45 surface markers and have preserved their adipogenic and osteogenic potential according to Oil Red and Alizarin Red stains. BMSCs were propagated in T175 CELLSTAR cell culture flasks (660175, VWR™) using the Rooster Basal™-MSC (SU-005, RoosterBio®) media supplemented with Rooster Booster™-MSC (SU-003, RoosterBio®) to create a master cell bank for each donor. All cells were certified mycoplasma-free and cultured in a humidified incubator (37°C, 5% CO_2) with cell culture media changes every 3 days. Cells retrieved from the cell bank were cultured in DMEM (D5796, Thermo Fisher) supplemented with 10 fetal bovine serum (FBS) (F0926-50ML, Sigma-Aldrich) and 1% penicillin/streptomycin solution (P/S) (P4333-100ML, Sigma-Aldrich). Cells were harvested at 75%–80% confluence after 7–8 days in culture using TripLE select (12563-029, Thermo Fisher).

2.4 | Cell adhesion

Untreated TCP and HEP/COL coated substrates were tested for cell adhesion by employing serum-free media formulations during a short incubation period. Bovine serum albumin (BSA) (A9647-50G, Sigma-Aldrich) was used to block cells from non-specific binding. A 30 μL volume of BSA 5% w/v in 1X DPBS was added to each culture well of a 96-well plate and incubated overnight at 37°C. Control conditions included BSA-free TCP surfaces. BSA-blocked surfaces were washed twice with 200 μL of 1X DPBS. BMSCs were seeded at a cell density of 10,000 cells/cm^2 in a serum-free media formulation composed of DMEM +1% P/S supplemented either with 5 mM $MgCl_2$ (63069-100ML, Sigma-Aldrich) or 5 mM Ethylenediaminetetraacetic acid (EDTA) (03690-10ML, Sigma-Aldrich). After a 4 h incubation period, wells were washed twice with DPBS to remove loose cells and fixed with 100 μL volume per well of 4% paraformaldehyde solution (PFA) (sc-281692, Santa Cruz Biotechnology) at room temperature (RT) for 10 min. A Hoechst 33342 (H3570, Thermo Fisher) nuclear stain was done by a 15 min incubation using a 100 μL volume per well at a 1:1000 ratio. Images at a 2X magnification were obtained with a fluorescence microscope (BZ X810, KEYENCE). Total cell counts were obtained from fluorescent micrographs using free-license ImageJ software.

2.5 | Quantification of integrin expression levels

The Alpha/Beta Integrin-Mediated Cell Adhesion Array Combo Kit, fluorimetric (ECM535, Sigma-Aldrich) was used to assess integrins expression by MSC as suggested by the vendors' protocol. Briefly, 10,000 cells/well were seeded on respective α and β integrin array plates using DMEM supplemented with 10% FBS. After 2 h incubation, unbound cells were washed away, and the adherent cells were lysed and labeled with provided CyQuant GR dye. Finally, culture plates were examined using a plate reader (Infinite® 200 PRO, TECAN) at 485 nm Ex. and 530 nm Em.

Flow cytometry analysis was used for integrins expression; for this, cells were harvested from culture using TripLE select. MSCs were

washed with 10 mL DPBS, treated with 3 mL TripLE select, and transferred to the incubator at 37°C for 5 min. Cell suspensions were mixed with 10 mL culture media, transferred to Corning® 50 mL centrifuge tubes (CLS430290, Sigma-Aldrich), and centrifuged at 300 *g* for 5 min for pellet formation and supernatant aspiration. Cells were resuspended in 3 mL 4% PFA and left at room temperature (RT) for 20 min. Next, cells were centrifuged at 300 *g* for 5 min to securely discard the supernatant and continue with cell resuspension in 3 mL 90% (vol/vol) cold methanol for additional 15 min incubation at 4°C. For methanol removal, cells were washed and centrifuged twice for 10 min and RT with 20 mL of 5% w/v BSA in DPBS (FlowBuffer). Sample pellets were resuspended in 2 mL fresh DPBS to estimate cell density based on cell counts. So, 1 million cells were transferred to microcentrifuge tubes with 100 μL of FlowBuffer containing appropriate primary antibodies concentration; mouse anti-α2β1 (ab30483, Abcam) or mouse anti-αvβ3 (MAB1976, Sigma-Aldrich) at a 1:250 dilution incubated for 1 h at RT. Cells were washed twice with DPBS and resuspended in 100 μL of FlowBuffer with Alexa-fluor 488 goat anti-mouse secondary antibody (A211121, Thermo Fisher) at a 1:1000 dilution for 30 min in the dark. Two final washes were done, then samples were resuspended in 300 μL of FlowBuffer and kept on ice before the assessment of integrins expression across donors using a flow cytometer tool (BD Accuri™ C6 Plus Cell Analyzer, BD Bioscience) equipped with the BD Accuri™ C6 Plus Software (BD Bioscience) for data analysis.

2.6 | Immunofluorescence staining

Chambered coverglasses (Nunc™ Lab-Tek™ 155361 Thermo Fisher) were coated with HEP/COL and drop-cast COL. COL drop-casting was done by letting 50 μL of COL solution dry over the glass surface for 6 h in a sterile environment. Cells were seeded at a density of 5000 cells/cm^2 on untreated and surface-modified coverglasses. After 3 days of culture, cells were fixed with a 4% PFA solution and permeabilized with 0.2% Triton X-100TM (10591461, Thermo Fisher) in DPBS for 10 min each at RT. Wells were rinsed three times with a washing solution composed of 1X DPBS + 0.1% Tween 20 (P9416, Sigma-Aldrich) after every single process. Samples were then blocked using 1% BSA diluted in washing solution for 1 h at RT. Integrins were stained using either mouse anti-α2β1 (Abcam) or mouse anti-αvβ3 (Sigma-Aldrich) at a 1:250 dilution for overnight incubation at 4°C. The secondary antibody, Alexa-fluor 488 goat anti-mouse (Thermo Fisher), was used at 1:200 dilution and a 2 h incubation period at RT.

For FAK and ERK½ staining, the primary antibodies rabbit anti-phosphorylated Y397 FAK (ab81298, Abcam) (pFAK) and rabbit anti-phosphorylated (T202/Y204) ERK½ (ab223500, Abcam) (pERK½) were used at a 1:100 dilution and overnight incubation at 4°C. An Alexa 647 goat anti-rabbit (ab150079, Abcam) was used as a secondary antibody at a 1:200 dilution and 2 h incubation period at RT. Wells were washed three times with 1X DPBS between antibody incubation periods. ActinGreen™ 488 ReadyProbes™ Reagent (R37110, Thermo Fisher) or ActinRed™ 555 ReadyProbes™ Reagent (R37112, Thermo Fisher) were used for labeling the cell cytoskeleton following the manufacturer's protocol. Hoechst 33342 diluted at a 1:1000 ratio was used to mark nuclear DNA. Fluorescent images were obtained at a 100X magnification using the fluorescence microscope BZ X810.

For endogenous cell-secreted COL immunolabeling, MSCs were seeded at 5000 cells/cm^2 in chambered coverglasses presenting four different culture substrates; glass, drop-cast COL, and HEP/COL substrates ended in COL (8-L) and in HEP (9-L). Immunostaining was performed at 48 h. First, cells were fixed with 4% PFA solution, and samples were blocked with 1% BSA diluted in washing solution. For COL labeling, a 1:200 dilution of rabbit anti-collagen 1 (ab138492, Abcam) was employed for 8 h at 4°C, followed by a 2 h incubation at RT with the Alexa 594 goat anti-rabbit (ab150084, Abcam). The cell nuclei were stained with Hoechst (1:1000 dilution). Fluorescent micrographs were captured at a magnification of 40X using the BZ X810 equipment. Images processing was done with ImageJ software after quantifying cells' fluorescence intensity per condition.

2.7 | Western blot

Cells were seeded at 12,000 cells/cm^2 on 12-well plates (Costar-3512, Corning) and cultured in DMEM supplemented with 2% fetal bovine serum and 1% P/S. After 24 h incubation, cells were lysed for 5 min using RIPA buffer (R0278, Sigma-Aldrich) with 10% protease and phosphate inhibitor (K271-500, BioVision) at RT. Cell lysates were transferred to 2 mL microtubes, centrifuged at 10,000 *g* for 10 min, and the supernatant was stored at −80°C. Total cell protein content was quantified using Qubit® Protein Assay Kit (Q33211, Thermo Fisher) according to the manufacturer protocol. Total protein content was adjusted to a concentration of 5 mg/mL, and samples were denatured by heat (70°C for 15 min) and separated through gel electrophoresis using a Blot 4%–12% Bis-Tris plus (Invitrogen™, NW04125BOX). The gels were then transferred onto iBlot 2 PVDF mini stacks (Invitrogen™, IB24002) and sequentially blocked (1 h) and incubated with either anti-FAK (ab76496, 1:1000 dilution), anti-ERK½ (ab17942, 1:1000 dilution), anti-phosphorylated Y397 FAK (ab81298, 1:1000 dilution), or anti-phosphorylated (T202/Y204) ERK½ (ab223500, 1:400 dilution) primary antibodies for 12 h at 4°C. Beta-actin protein band was used as a sample loading control and stained with Rabbit anti-β-actin (ab8227, Abcam) at a 1:1000 dilution. Finally, samples were incubated for 1 h with horseradish peroxidase-labeled (HRP) goat anti-rabbit secondary antibody (ab6721, Abcam, 1:2000 dilution) followed by 10 min incubation with Luminol (c-2048, Santa Cruz Biotechnology). Chemiluminescent signals from each protein were imaged and analyzed employing the ChemiDoc XRS+ instrument (Bio-Rad) and Image Lab software (Bio-Rad) to calculate relative protein band levels.

2.8 | Integrin and ERK½ inhibition

BTT-3033 (4027, TOCRIS, place) and Cilengitide (SML1594-5MG, Sigma Aldrich), are selective inhibitors against α2β1 and αvβ3 integrins, respectively. SCH772984 (10380, ACHEMBLOCK) was used as a pharmacological inhibitor for ERK½. For cell viability, BMSCs at a seeding density of 10,000 cells/cm^2 were cultured for 48 h in DMEM supplemented with 2% FBS, 1% P/S, and incremental dosages for specific inhibitors against α2β1, αvβ3, and ERK½ using black wall 96-well plates (655090, Sigma-Aldrich). A 7-point dose–response curve was used to calculate the IC_{50} values. The concentrations ranged from 0 to 218 μM with six 9-fold logarithmically spaced concentrations in between for BTT-3033 and Cilengitide; whereas for SCH772984, concentrations ranged from 0 to 2.6 μM based on vendors' specifications. After incubation, culture media was replaced by a 10% v/v solution of PrestoBlue™ cell viability reagent (A13261, ThermoFisher Scientific) diluted in fresh media and incubated for an additional 40 min at 37°C and 5% CO_2. Cell viability was then measured using the Infinite® 200 PRO plate reader at 560 nm Ex. and 590 nm Em. GraphPad Prism was used to analyze the collected data and create drug response curves from non-linear regression analyses providing values for half and three-quarters inhibitory concentrations (IC_{50} and IC_{75}).

2.9 | Cell proliferation

The quantity of proliferating cells from cultures on plastic and HEP/COL surfaces were evaluated using the Invitrogen Click-iT EdU Alexa Fluor 647 Imaging Kit (C10340, Thermo Fisher). BMSCs were seeded on 96-well plates at 10,000 cells/cm^2 using DMEM supplemented with 2% FBS and 1% P/S for 3 days employing either BTT-3033, Cilengitide, or SCH772984 at detected IC_{50} and IC_{75} dosages. For cell labeling, cultures were treated with 10 μM Edu stock solution for 12 h; next, cells were fixed and permeabilized for 20 min each with 4% PFA and 0.2% Triton X-100TM. Wells were washed twice with 200 μL of 3% BSA in DPBS and treated with 100 μL of EdU reaction cocktail consisting of 1X Click-iT® EdU reaction buffer (21.4 mL), $CuSO_4$ (1 mL), Alexa Fluor® azide (62 μL), and 1X Click-iT® EdU buffer additive (2.5 mL), for 30 min protected from light at RT. Finally, all samples were washed with DPBS and treated with Hoechst 33342 for 15 min to dye the whole cell population. Fluorescent images were taken at a 10X magnification using the BZ X810 equipment. Cell counts were acquired from fluorescent micrographs through ImageJ software.

2.10 | Cell apoptosis

The number of apoptotic cells from cultures treated with either BTT-3033, Cilengitide, or SCH772984 was studied using fluorescently labeled Annexin V protein (640906, BioLegend) and Propidium Iodide (PI) (CS1-0109-5mL, Nexcelom). BMSCs were grown for 5 days on HEP/COL substrates using detected IC_{50} and IC_{75} dosages for inhibiting α2β1, αvβ3, and ERK½. Cell monolayers were treated with Annexin V/PI (1:1000) in Annexin V binding buffer for 10 min for cell labeling. After that, samples were fixed for 15 min using 4% PFA and washed twice with DPBS. Cell nuclear dyeing was done with Hoechst for 10 min. Finally, cells were washed twice, and images were captured at 10X magnification using the BZ X810 microscope. Cell counts were acquired from fluorescent images using the ImageJ software.

2.11 | Macrophage inhibitory assay

The Bio-Plex Pro™ Human Cytokine 27-plex Assay (M500KCAF0Y, BioRad) was used to assess the macrophage polarization potential, building upon a previously reported THP-1 assay.[30] In this regard, THP-1 monocytes were cultured in HEP/COL-coated 96-well plates, either individually or in co-culture with MSCs at a 1:10 ratio of MSC to THP-1. Control wells with no MSCs (THP-1 only) or no THP-1 cells (MSCs only) were also included. MSCs were seeded first, either with or without IC_{50}, and IC_{75} detected dosages for BTT-3033 and allowed to adhere for 12 h before adding 200 μL of RPMI medium supplemented with 10% FBS and THP-1 cells. The cells were then cultured overnight and treated with 1 μg/mL lipopolysaccharide (LPS) for 6 and 24 h before media collection for multiplex analysis. Briefly, 50 μL of collected media and standards were mixed with magnetic beads dissolution and incubated at RT and ~850 rpm for 30 min. Following this, the plate underwent three washing steps using the BioPlex Handheld Magnetic Washer (171020100, BioRad). Next, 25 μL of detection antibodies were added to each well, and the plate was protected from light while being shaken at ~850 rpm for a 30 min incubation at RT. After washing, 50 μL of streptavidin-PE was added to each well and incubated for 10 min with shaking. The beads were then resuspended in 125 μL of assay buffer and shaken for 30 s at ~850 rpm. Using low PMT and RP1 settings, the assay plate was analyzed in a Bio-Plex® 200 System (BioRad). The collected data was then processed using Bio-Plex Manager™ version 6.2 (Bio-Rad Laboratories, Inc.). Results were reported as median fluorescence intensities (MFI) and the concentration of detected cytokines (pg/mL).

2.12 | Statistical analysis

Experiments were duplicated with an $n = 3–5$ per treatment. Results are presented as mean ± standard error of the mean (SEM). A two-way analysis of variance (ANOVA) was done to detect significant changes for multifactorial analysis. Statistical analysis was performed using Graph Pad Prism 7.0 software for Windows. A p-value <.05 was considered statistically significant.

3 | RESULTS

3.1 | HEP/COL multilayers physicochemical characterization

HEP and COL layers were sequentially deposited on TCP as a multi-stack of single alternating layers using oppositely charged (HEP,

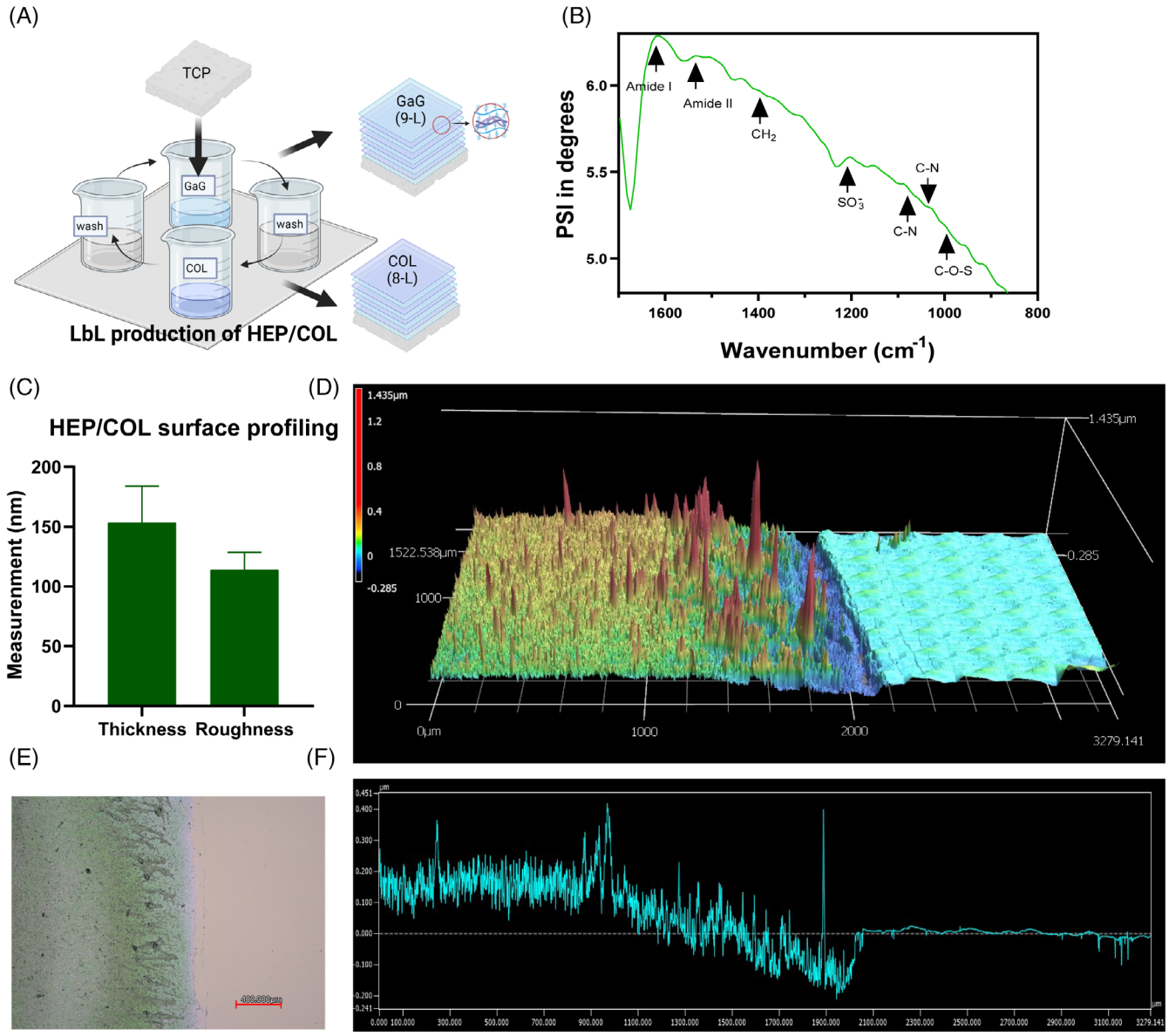

FIGURE 1 HEP/COL deposition process and layers characterization. (A) LbL surface modification to generate COL- (8-L) and HEP-ended (9-L) HEP/COL substrates. This figure was created with BioRender.com. (B) IR-VASE Spectrum of surface-deposited HEP/COL (9-L). (C) Bar graph shows the thickness and roughness analysis of surface-deposited HEP/COL (9-L). Data represents the mean ± SEM of $n = 3$ samples. (D) Three-dimensional illustration of HEP/COL bilayers on the top of a silicon substrate. (E) Optical micrograph displaying a high-magnification view of a silicon substrate coated by HEP/COL on one half (left side). (F) Surface profile of scanned areas from Panel (D).

charged negatively, and COL with a positive charge) polymeric solutions analogously to what was described by Decher et al.[31] Figure 1A shows a graphical representation of the layer-by-layer (LbL) surface deposition method used to generate cultures surfaces containing either 8 (8-L) and 9 (9-L) single total layers corresponding to COL-ending and HEP-ending surface coatings, respectively. Positively charged culture surfaces are exposed to a negatively charged HEP solution, followed by a washing step in acetate buffer and the COL deposition using a positively charged COL-based solution. This cyclic process is then repeated 8 or 9 times to get COL-ending or HEP-ending surface bilayers. A minimum of eight bilayers is used to ensure full surface coverage on tissue-culture-treated plastic, as we described before.[21]

Analogous steps were used to deposit HEP/COL onto silicon wafers for subsequent physicochemical characterization. The existence of the distinctive collagen I triple helix and heparin structures was confirmed by the different functional groups' amide I (1700–1600 cm^{-1}) and amide II (1600–1500 cm^{-1}) being discernible within the built layers[21] (Figure 1B). Additionally, characteristic peaks were located in agreement with the literature, such as the CH_2 scissoring peak surrounding 1400 cm^{-1}, the C N stretching at 1070 and 1040 cm^{-1}, and the C O S stretching vibrations at around 950 cm^{-1}.[29] These results confirm the deposition of HEP/COL onto silicon wafers. Multilayer thickness and surface roughness had an average thickness of 150 nm and a corresponding surface roughness

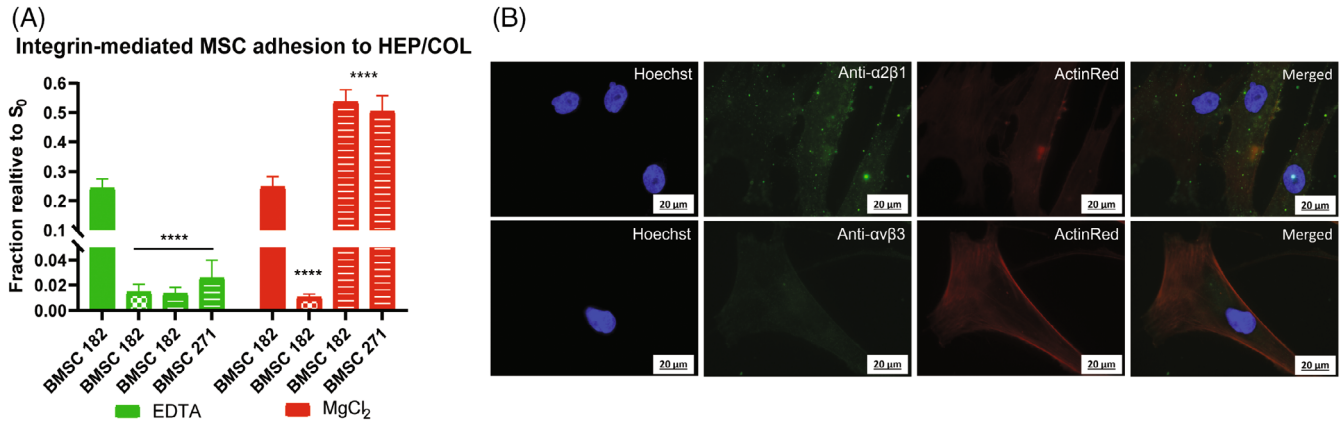

FIGURE 2 MSCs expressed integrins and their binding affinity to LbL-produced HEP/COL substrates. (A) MSCs adhesion at 4 h to TCP (solid bars), BSA-blocked plastic (square bars), and (9-L) HEP/COL multilayers (striped bars) in the presence of EDTA or $MgCl_2$. Two-way ANOVA was used for statistical analysis among conditions. (*) Significantly different than TCP without BSA blocking; $n = 6$, $^{****}p \leq .0001$. (B) MSC's expression of α2β1 and αvβ3 as detected by immunofluorescence (blue = nuclei, green = integrins, and red = actin fibers) for α2β1 and αvβ3 integrins, scale bar 20 μm.

of approximately 110 nm (Figure 1C). These findings align with our prior ellipsometry-based results, which also indicated a thickness and roughness of about 100 nm.[21] Figures 1D,E display representative images of a 3D map constructed from a scanned area of approximately 3000 × 1000 μm^2 and an optical micrograph taken at 5X magnification. Additionally, Figure 1F provides a 2D cross-section representation of the roughness profile, emphasizing the average differences between the peaks and valleys within the scanned region.

3.2 | HEP/COL multilayers promote cell adhesion via integrin activity

Integrin-mediated cell adhesion was manipulated by adding $MgCl_2$ or EDTA to serum-free media formulations. The rationale behind this assay comes from the need for Mg^{2+} cations to support integrin-mediated adhesion to COL,[32] while EDTA will block this interaction by sequestering Mg^{2+} ions.[33] As expected, $MgCl_2$ and EDTA treatments did not significantly affect cell adhesion to TCP, as shown in Figure 2A (solid bars), being consistent with a non-integrin-dependent cell binding mechanism. TCP surfaces blocked with BSA (squared bars), used as a negative control for cell adhesion, did not support cell attachment regardless of EDTA and $MgCl_2$ treatments. On the other hand, the number of cells bound to HEP/COL surfaces (striped bars) was supported by the presence of Mg^{2+} in media and significantly decreased in the presence of EDTA, consistent with an integrin-dependent cell adhesion mechanism.

Owing to the high rates of MSC adhesion mediated by integrin binding on HEP/COL substrates, we then profiled the expression levels of αβ-binding integrins in MSC cultivated on α and β monoclonal antibodies arrays (Supplementary Figure S1). Results show that MSCs adhered to most integrin subunits and dimeric conformations, but the abundance differs across donors. While all integrins were expressed in donor BMSC 271, integrins β3, β4, and β6 single subunits were not detected in donor BMSC 182 (Figure S1).

Among the integrins expressed in these MSC donors, we centered our attention on the study of α2β1 and αvβ3 integrins, in light of their association with the cell cycle progression.[34,35] In addition, α2β1 rather than αvβ3 stimulation is directly related to COL binding motifs.[36] Thus, examination of αvβ3 will serve as a treatment group to distinguish among processes mediated by collagen-integrin interactions versus other integrin activities generated by biomolecules present in the serum and secreted by cells.[37] The presence and abundance of the selected integrins were confirmed by flow cytometry (Figure S1) and immunofluorescence (Figure 2B), with a prevalence of more than 90% of the MSC population for both donors.

3.3 | HEP/COL multilayers enhance COL deposition and FAK-ERK½ activation in MSCs

Canonical α2β1 integrin-mediated adhesion to COL is associated with FAK-ERK½ signaling activity.[38] Therefore, increased collagen-integrin stimulation should lead to enhanced levels of FAK and ERK½ activation. The level of stimulation of FAK and ERK½ signaling was measured by comparing the expression magnitude of total and phosphorylated FAK and ERK½ in cells cultivated in HEP/COL, COL and TCP substrates. Protein blots for each donor are shown in Figure 3A,B, and intensity band quantifications are in Figure 3C–F. Remarkably, the levels of phosphorylated FAK and ERK½ were notably higher for HEP/COL surfaces relative to control conditions. The enhanced FAK-ERK½ activity was consistent across both donors. Immunofluorescent staining of phosphorylated FAK-ERK½ visually confirmed enhanced phosphorylation intensity on HEP/COL relative to controls (Figure 4). Interestingly, the fluorescence staining reflected higher FAK-ERK½ proteins phosphorylation on HEP/COL than surfaces coated with COL alone, indicating that the presence of HEP is

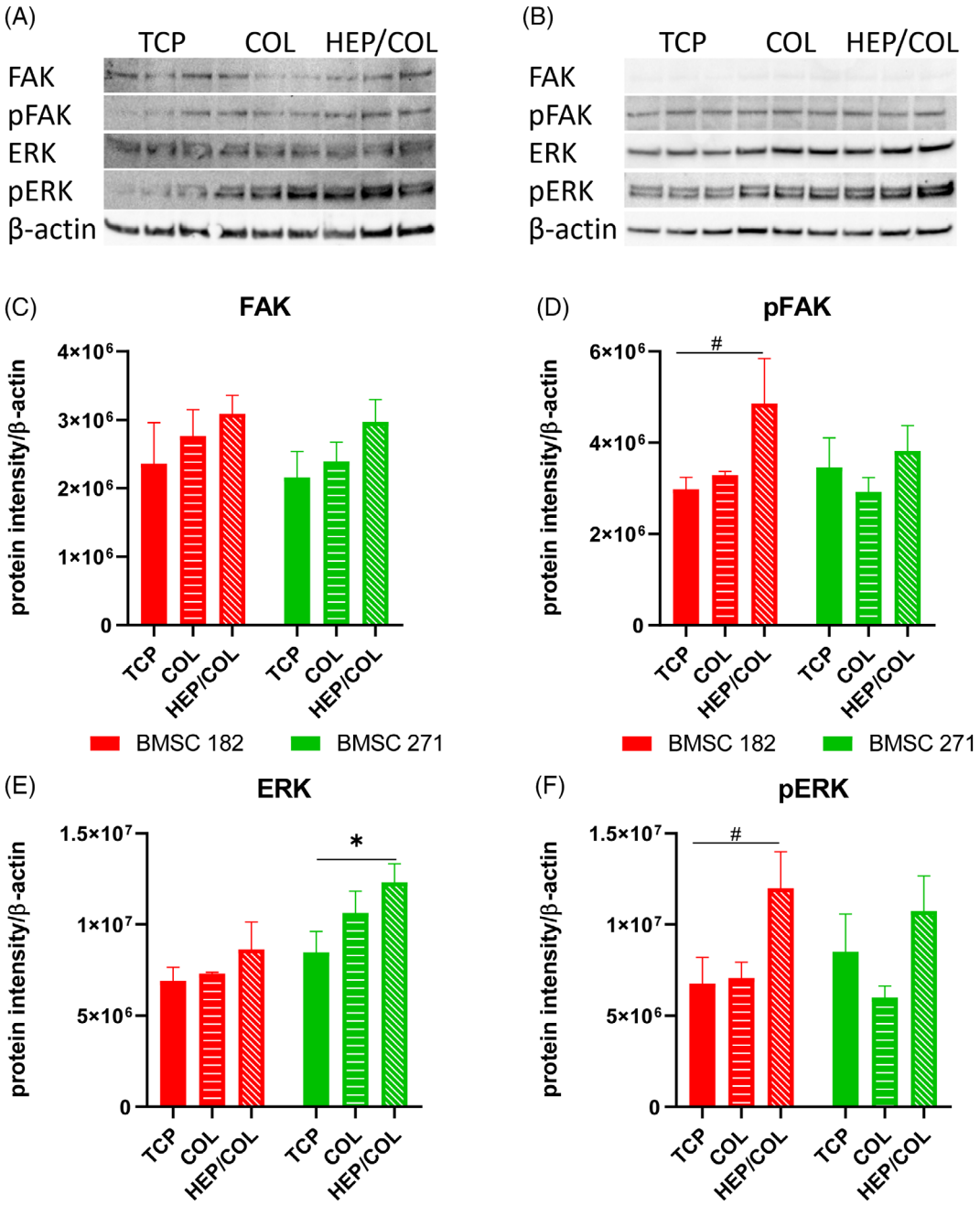

FIGURE 3 HEP/COL enhances the activation of FAK and ERK½ in MSCs. Protein bands for FAK and ERK½ from MSC cultured for 24 h on plastic, COL and (9-L) HEP/COL surfaces for (A) donor BMSC 182 and (B) BMSC 271. Quantification levels for (C) FAK, (D) phospho-FAK, (E) ERK½, and (F) phospho-ERK½ from MSCs (both donors) cultured on plastic, COL, and HEP/COL. Unpaired *t*-tests were used for statistical analysis. (*) Significantly different than TCP (same donor); *$p \leq .05$. (#) Marginally significant $.05 < p \leq .1$. $n = 3–6$.

critical for the observed enhancements of FAK-ERK½ activity and underscores the potent signaling response elicited by the HEP/COL substrate.

One potential mechanism by which HEP can enhance integrin activity and consequently positively impact FAK-ERK½ activation is through increased endogenous COL deposition. Recent studies indicated that either heparin or heparan sulfates are necessary for early ECM fibril formation.[26] Moreover, MSCs naturally secrete COL, and in the presence of heparin, this is expected to be better retained on the culture surface due to the strong binding affinity among both proteins (kd value = ~60–80 nM).[39] To test for enhanced endogenous COL deposition, cultured cells were stained on uncoated glass, drop-cast COL, and HEP/COL surfaces ending in both COL (8-L) and HEP (9-L) after 48 h incubation. Figure 5A shows representative immunofluorescent images of COL stained in MSC cultures where HEP/COL ending in HEP (9-L) but not COL (8-L) shows significantly higher COL deposition relative to glass or COL drop cast (Figure 5B). These findings collective indicate that

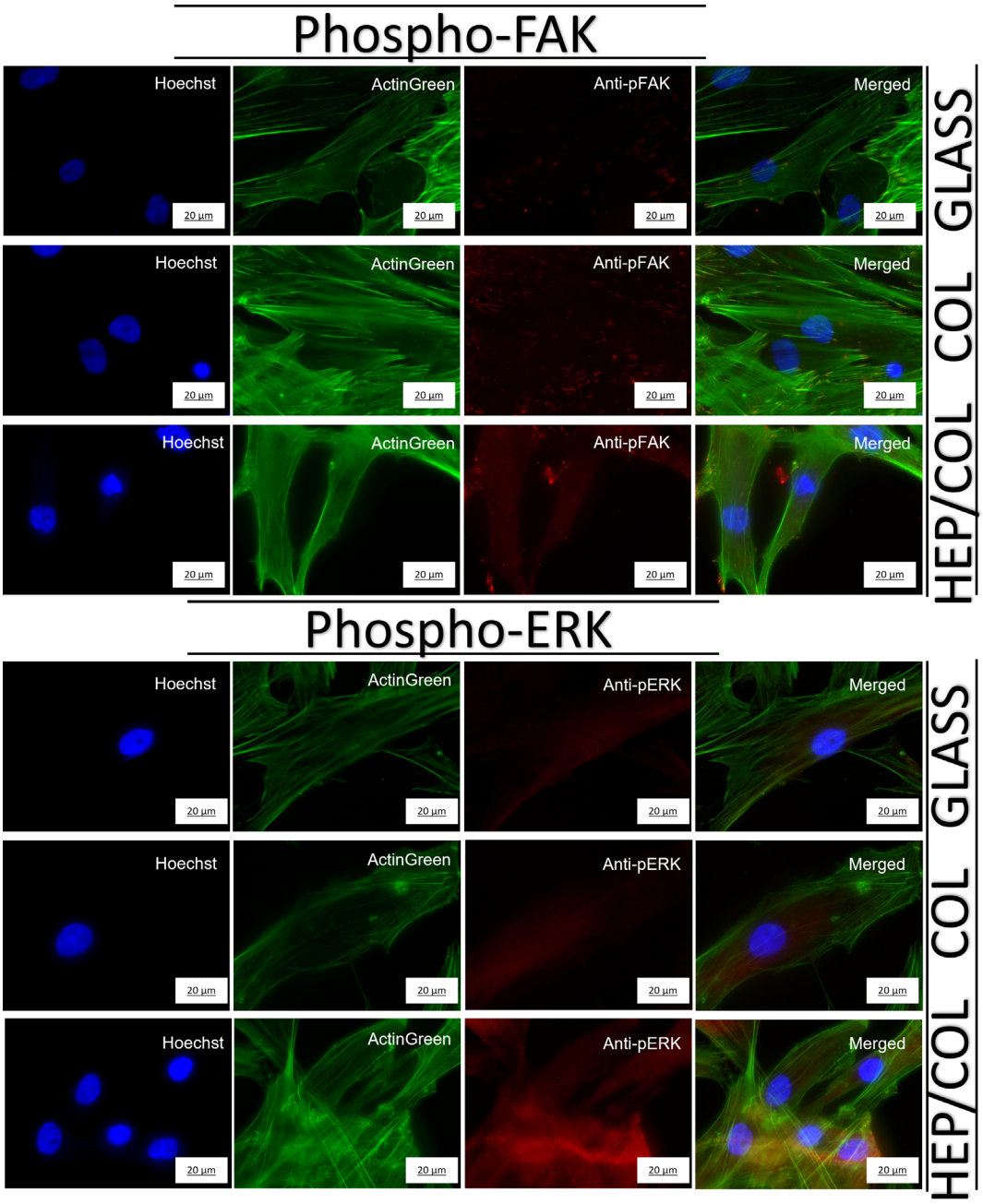

FIGURE 4 FAK and ERK½ activities are enhanced on HEP/COL surfaces. Fluorescent images from BMSCs cultured on glass, COL, and HEP/COL coatings showing the intensities of detected pFAK and pERK½ (blue = nuclei, red = phosphorylated proteins, and green = actin fibers). Scale bar = 20 μm.

HEP facilitates integrin signaling via promoting cell endogenous COL deposition.

3.4 | α2β1 promotes enhanced FAK and ERK½ signaling activity on HEP/COL multilayers

To determine the role of COL integrins in the observed enhanced activity of FAK and ERK½, we performed cellular studies using pharmacological inhibitors selective for α2β1 (COL integrin) and αvβ3 (non-COL integrin). Inhibition of α2β1, using BTT-3033, showed a significant drop in the number of adhered cells to HEP/COL (Figure 6A). On the other hand, inhibition of αvβ3 did not reduce the number of attached cells compared to untreated control conditions, indicating that this integrin has a less prominent role in regulating cell adhesion to HEP/COL. In agreement with these findings, the total and phosphorylated levels of FAK and ERK½ protein bands were notably reduced by BTT-3033 treatment at concentrations of 2.69 μM or higher in cells cultured on HEP/COL multilayers (Figure 6B–G). A decreasing linear trend was observed as the BTT-3033 concentration was increased for both MSC

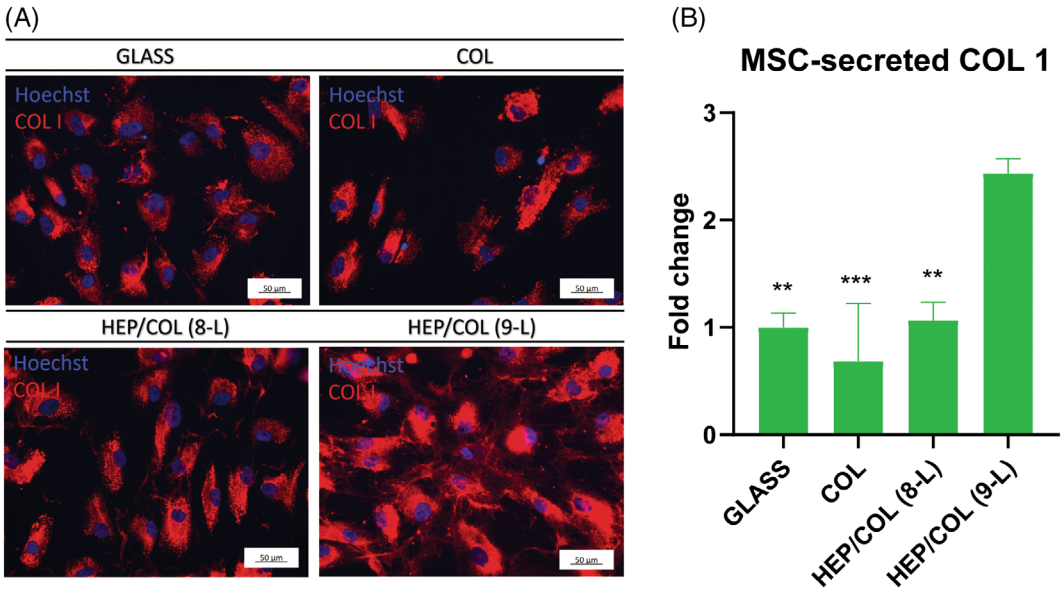

FIGURE 5 Endogenous COL deposition is enhanced on HEP/COL surfaces. (A) Fluorescent images of BMSC 271 stained for COL after 48 h incubation period on glass, COL, and HEP/COL coated surfaces (8-L and 9-L) (blue = nuclei, red = secreted COL). Scale bar 50 µm. (B) Quantification of COL intensity per surface area across culture surfaces. Data represents the average of the mean intensity value ± SEM, with $n = 3$ images containing 10–22 cells per picture. Statistical analysis by One-way ANOVA. $^{**}p \leq .01$; $^{***}p \leq .001$.

donors. Cells treated with SCH772984, an ERK½ inhibitor, showed decreased ERK½ phosphorylation levels without affecting total and phosphorylated FAK levels (Supplementary Figure S2), confirming that ERK½ phosphorylation occurs downstream of FAK on HEP/COL substrates. BTT-3033 treatment also decreased FAK and ERK½ protein bands in TCP. Yet, these effects were ~ 3 orders of magnitude lower than on HEP/COL multilayers and consistent with the low integrin engagement levels associated with cell adhesion on this culture surface. Inhibition of αvβ3 using Cilengitide showed no appreciable effect in FAK or ERK½ levels (Figure 7), confirming that this integrin is not involved in the enhanced FAK and ERK½ activity levels noticed in cells cultured on HEP-ending HEP/COL surfaces.

3.5 | α2β1 activity supports enhanced cell viability on HEP/COL multilayers

Cell growth, viability, and apoptosis were evaluated to determine the impact of enhanced COL integrin activity via FAK-ERK½ on the survival and expansion of MSCs on HEP/COL surfaces. Initial viability evaluations were performed on MSC capacity to metabolically reduce resazurin to resorufin using a 7-point dose–response curve for each pharmacological inhibitor of αvβ3, α2β1, and ERK½. The collected data were processed via non-linear regressions to compute the IC_{50} and IC_{75} dosage values for each compound across both donors (Figure 8A). Results on cell apoptosis at the IC_{75} values are summarized in Figure 8B,C. In general, treatments with each inhibitor increased cell apoptosis; however, BTT-3033 treated cells showed significant impairments relative to control conditions in both donors emphasizing the essential role of α2β1 activity in promoting cell survival on HEP/COL substrates. Cilengitide treatment showed statistical significance for one donor, and marginal significance in the other, indicating that αvβ3 activity also contributes to increased cell apoptosis. As expected, cell apoptosis was not significantly affected at the IC_{50} doses (Supplementary Figure S3A), which is consistent with the high phosphorylation levels of FAK and ERK½ observed at equivalent IC_{50} values but not at or above the IC_{75} value (Figure S4 and Figure 6), further supporting a mechanism driven by α2β1/FAK/ERK½ signaling cascade.

Cell growth was examined based on total cell quantifications and the fraction of cells in the S-phase. In agreement with our prior studies,[21] total cell yields were significantly higher for cells on HEP/COL than for those cultures on COL and TCP (Figure S3B,C). Examination of the fraction of cells in S-phase further confirms enhanced cell growth rates on HEP/COL relative to COL-coated and TCP surfaces (Figure S3D). Investigation of pharmacological inhibitors of integrins and ERK½ at both IC_{50} and IC_{75} dosages did not significantly alter the proportion of cells in the S-phase on HEP/COL surfaces (Figure S3E,F), confirming that α2β1 integrin activity is implicated in the retention and increased cell viability that, in turn, supports higher cell yields rather than altering the cell growth rates.

3.6 | α2β1 activity supports MSC immunomodulatory potency on HEP/COL multilayers

Inhibitory assessments of the M1 phenotype polarization in monocytes mediated by MSCs were done on HEP-ending surface bilayers

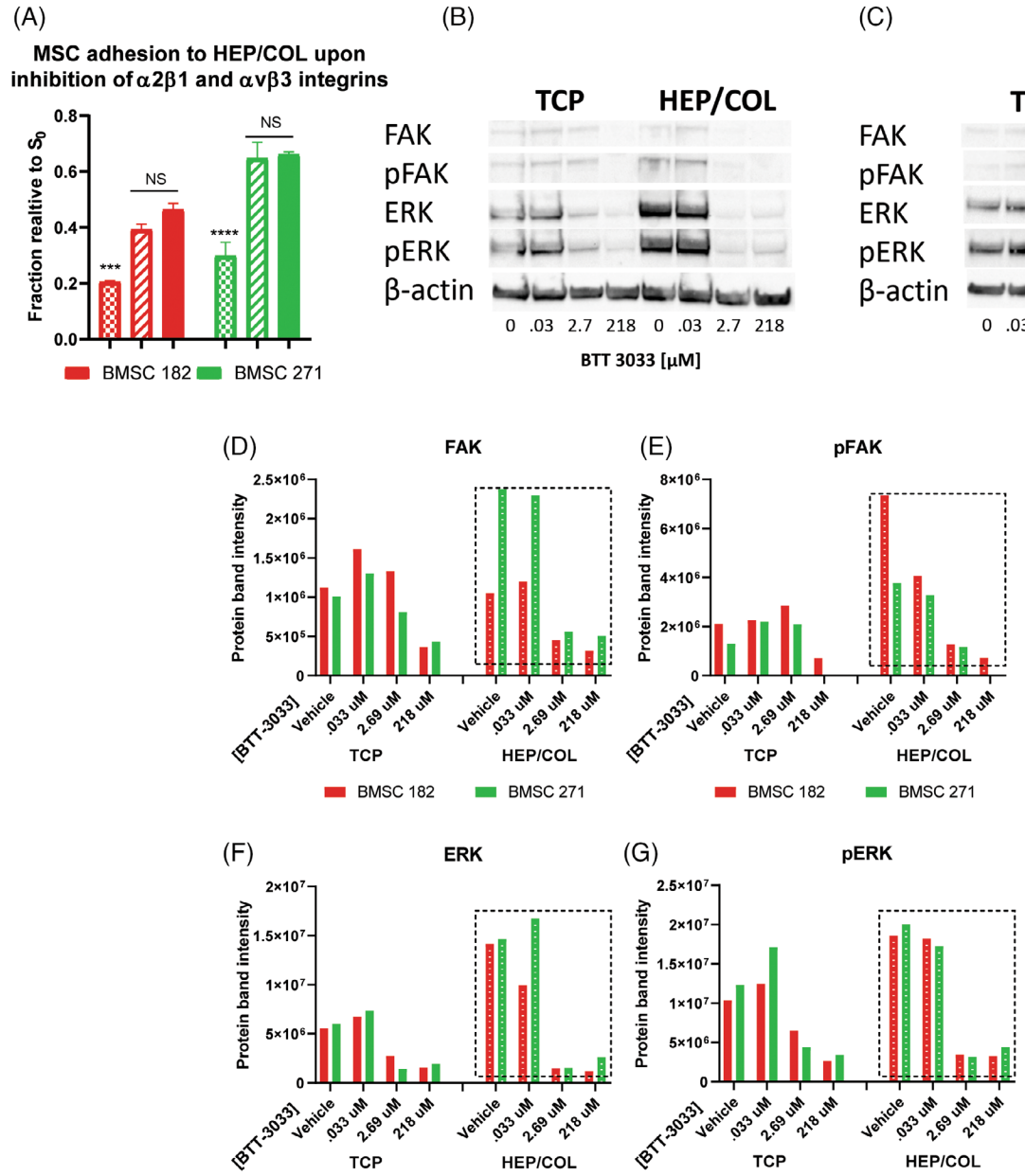

FIGURE 6 Integrin α2β1 promotes cell adhesion to HEP/COL and enhances FAK-ERK½ activity. (A) MSC adhesion to HEP/COL after 4 h in the presence of $MgCl_2$ (solid bars) treated with pharmacological inhibitors of α2β1 (square bars) and αvβ3 integrins (striped bars). IC_{50} concentrations of both inhibitors, derived from non-linear regressions (Figure 8), were used for this assessment. Two-way ANOVA was used for statistical analysis among conditions. (*) Significantly different than HEP/COL with no inhibitors; $n = 3$, ***$p \leq .001$; ****$p \leq .0001$. FAK and ERK½ protein bands from (B) donor BMSC 182 and (C) BMSC 271 in response to BTT-3033 treatment. (D–G) Plotted protein intensity band levels of total and phosphorylated FAK (D, E) and ERK½ (F, G) for two MSC donors treated with BTT-3033 for 24 h. Dashed squares highlight protein band levels on HEP/COL multilayers.

to determine the impact of α2β1 integrin activity on the immunomodulatory potency of MSCs (Figure 9A). The deliberate choice of a 1:10 ratio of MSC to THP-1 in our in-vitro co-cultures aimed to replicate the inflammatory milieu typical of specific pathological conditions.[40,41] This decision is further substantiated by multiple established studies that consistently utilize the same MSC to THP-1 ratio.[30,42,43] Cytokine levels in conditioned media derived from monocultures and co-cultures revealed that MSCs alter the macrophage secretory profile. MSCs monocultures did not show high levels of the majority of cytokines as compared to THP-1 in monoculture; however, the crosstalk between MSCs and monocytes synergistically upregulate the secretion of anti-inflammatory cytokines supporting the immunomodulatory activity of MSCs grown on HEP/COL substrates (Figure S5).

A total of eight cytokines were examined in response to IC_{50} and IC_{75} dosages of the α2β1 inhibitor BTT-3033. Specifically, INF-γ,[44,45] IL-6,[46,47] IL-10,[48] IP-10,[49] TNF-α,[50] MCP-1,[51] PDGF-bb,[52] and IL-8[53]

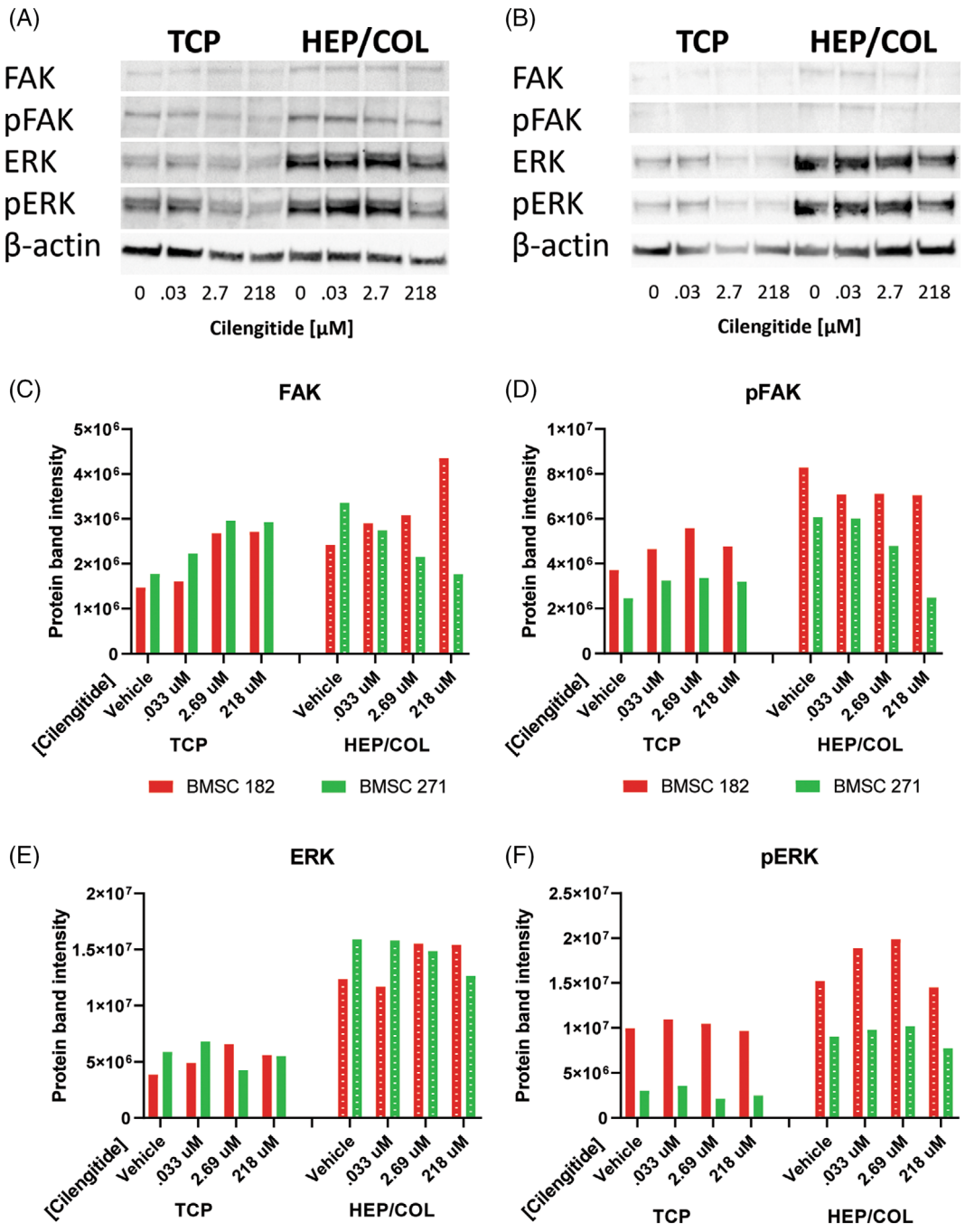

FIGURE 7 FAK-ERK½ levels are not affected by αvβ3 inhibition. FAK and ERK½ protein bands from (A) donor BMSC 182 and (B) BMSC 271 in response to Cilengitide treatment. (C–F) Plotted protein intensity band levels of total and phosphorylated FAK (C, D) and ERK½ (E, F) for two MSC donors treated with Cilengitide for 24 h.

cytokines were selected based on their reported immunomodulatory function in macrophages and other anti-inflammatory activities. The impact of integrin α2β1 inhibition on the immunomodulatory activity of MSCs is summarized in Figure 9B–I. Notably, IP-10, MCP-1, and TNF-α (Figure 9B–D) cytokines displayed a highly responsive behavior to increasing dosages of BTT-3033, exhibiting statistically significant differences in cytokine concentration within co-culture conditions. The increasing levels of TNF-α suggest that the efficacy of MSCs in suppressing monocyte polarization towards a pro-inflammatory M1 phenotype is diminished due to a reduction in α2β1 activity. IL-8 (Figure 9E) was shown to be slightly affected by the α2β1 inhibitor; however, the lack of statistical significance in the results precludes any conclusive statement regarding this effect. Neither INF-γ, IL-6, IL-10, nor PDGF-bb (Figure 9F–I) displayed any discernible impact after inhibiting the α2β1 integrin, indicating that only a subset of anti-inflammatory factors is affected by this integrin activity.

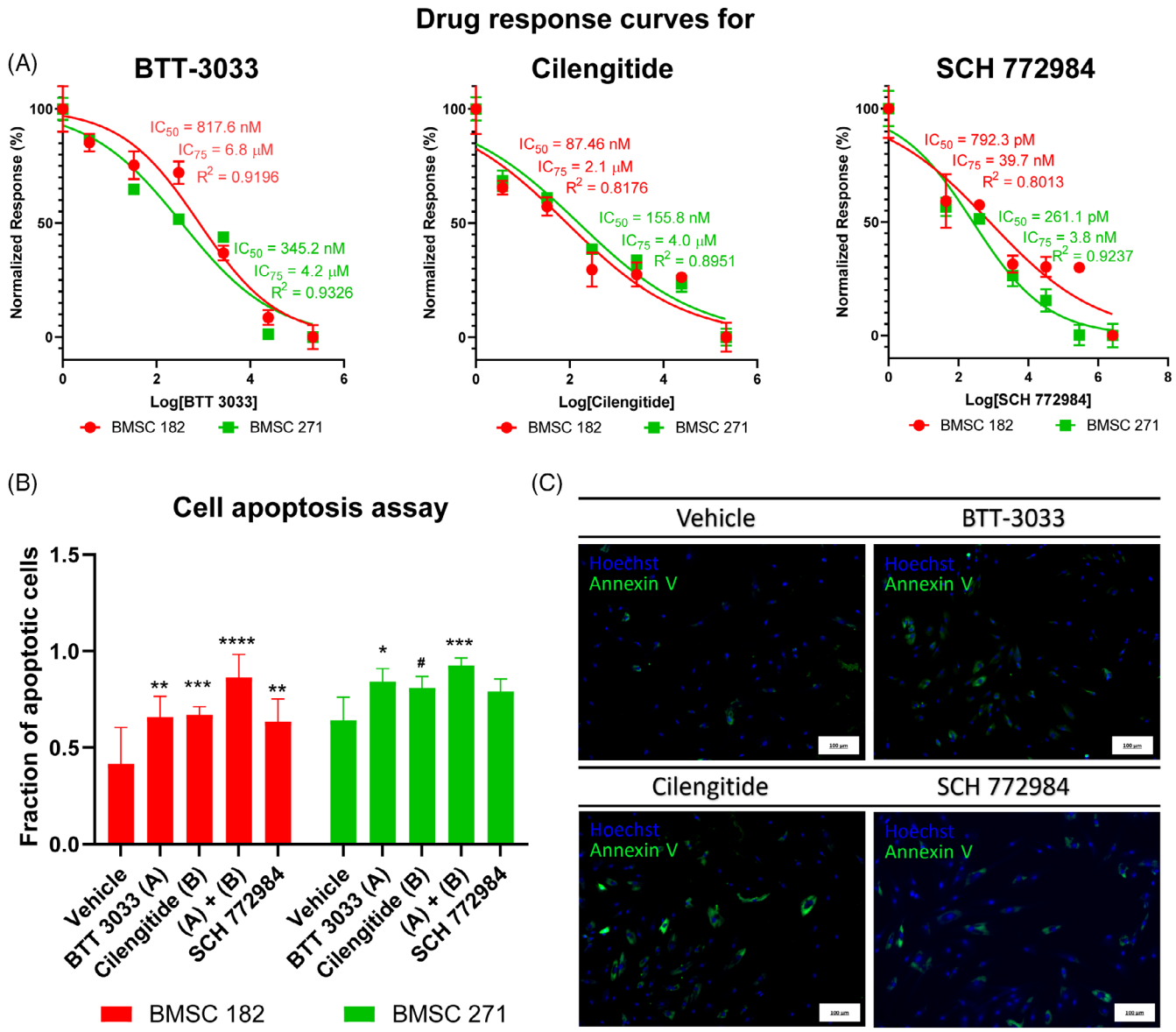

FIGURE 8 Integrin α2β1 supports MSCs viability on HEP/COL substrates. (A) Drug–response curves for MSCs (two donors) viability upon stimulation with incremental dosages of BTT-3033, Cilengitide, and SCH772984 on HEP/COL multilayers. Data were normalized between 0 and 100 and fitted by non-linear regression to identify specific IC_{50} and IC_{75} dosages. $n = 3$. (B) Fold change for Annexin V positive cells (donors BMSC 182 and 271) upon treatment with computed IC_{75s} for BTT-3033, Cilengitide, and SCH772984. Data represented the mean ± SEM of $n = 6$. Two-way ANOVA was used for statistical analysis. (*) Significantly different than vehicle; *$p \leq .05$; **$p \leq .01$; ***$p \leq .001$ (#) Marginally significant $.05 < p \leq .1$. (C) Representative images of apoptotic cells cultured on HEP/COL with and without drug stimulations, scale bar 100 μm.

These findings indicate that α2β1 activity is relevant for the anti-inflammatory potency of MSCs.

4 | DISCUSSION

The expansion of MSCs for therapeutic purposes requires cell-adherent culture substrates with environmental cues supportive of cell survival, growth, and potency.[6,54] Sulfated glycosaminoglycans (GAG) are abundant in the native tissue of the bone marrow[55] and represent an untapped potential for the in-vitro expansion of MSCs. GAGs, like HEP, possess a high affinity for hundreds of biomolecules and growth factors,[56] enabling the regulation of their release and prolonged stability in culture.[57] This is analogous to the function of heparin and other GAGs in tissues,[58] where growth factors signals and gradients are regulated by their participation in the bulk COL matrix.[59] However, heparin, as a single component, is unsupportive of robust cell adhesion,[60,61] limiting its applications in cell culture. Different studies employing HEP/COL for MSCs manufacturing have shown better outcomes for adhesion, growth, secretome, and senescence, among others,[21,22,62] but no specific mechanisms have been explored. Here, for the first time, we demonstrate that HEP and COL

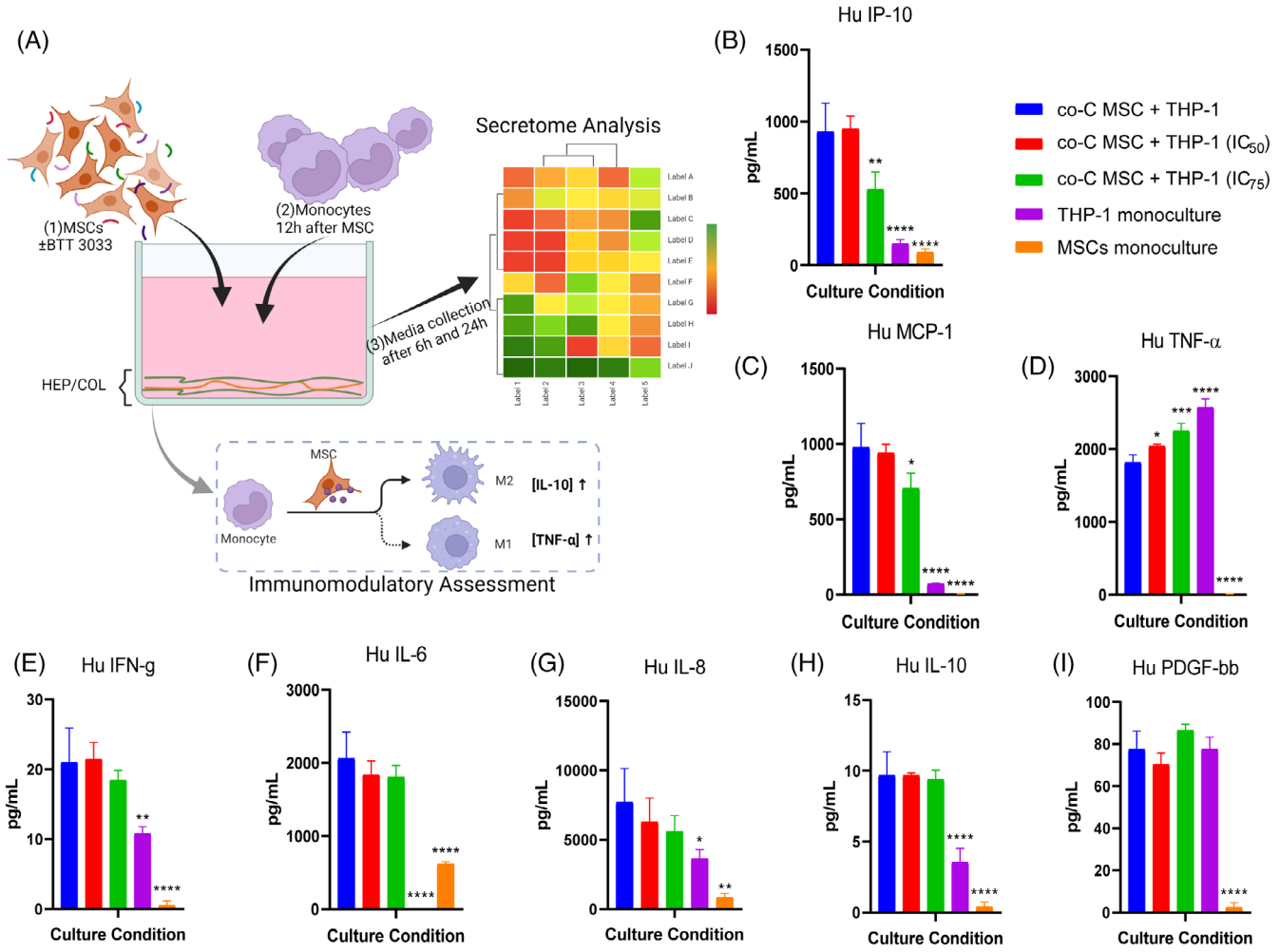

FIGURE 9 HEP/COL supports MSCs' immunomodulatory activity via α2β1 integrin activation. Summary of the cytokine profile from conditioned media derived from single cell monolayers and co-cultures after 6 h of LPS stimulation at 1 μg/mL concentration. (A) Shows a schematic representation of the potency assay used in this study. It illustrates how MSCs modulate THP-1 monocyte polarization towards an anti-inflammatory M2 phenotype. This figure was created with BioRender.com. Panels (B–I) summarize the cytokine levels after pharmacological inhibition of α2β1 integrin using BTT-3033. All factors were evaluated at 6 h except for TNF-α, which was examined at 24 h due to an increased significance at the 24 h mark. Data were normalized to the quantity of MSCs per condition and represented the mean ± SEM of $n = 3$. One-way ANOVA was used for statistical analysis. (*) Significantly different than co-C MSC + THP-1 conditions (blue bars); $^{*}p \leq .05$; $^{**}p \leq .01$; $^{***}p \leq .001$; $^{****}p \leq .0001$.

collaborate with α2β1 integrin to enhance cell growth, viability, and immunomodulatory potency via enrichments in the activity of the FAK-ERK½ signaling pathway. Thus, the combination of COL and HEP as bilayers rather than as individual components is more tissue mimetic, and the benefit is twofold: first, it enhances cell adhesion via integrin interactions preventing cell losses during culture, and second, it acts as a biomolecule reservoir where cell endogenous factors are sequestered and preserved by HEP leading to a more robust stimulation of integrins and reducing the need for frequent replenishment in cultures.

The benefits of α2β1 activity may be used to guide engineering approaches by shifting the current focus on RGD-integrins towards other structural COL integrin motifs. Of particular interest is GFOGER, as this motif is linked explicitly to the triple helix structure of COL present in the tropocollagen state. In fact, incorporating GFOGER over RGD into PEG hydrogels was shown to support MSC viability in-vitro, achieving cell yields with better engraftment and bone reparative activities.[63] In addition, other studies inspired by peptides in the COL triple-helix have been used to support cell adhesion and differentiation on scaffolds intended for tissue repair, drug delivery, and immunomodulation, among others.[64] By itself, GFOGER is not the only integrin-binding motif in COL; α2β1 can bind to other sequences like GMOGER and GLOGER, which are also present in fibrillar COL structures. Yet, these integrin binding motifs associated with the fibrillar structure of COL have been far less explored for cell culture applications due to their lower binding affinity towards α2β1 integrin relative to GFOGER-containing sequences.[65] However, because fibrillar collagens are more predominant in the native tissues, particularly the bone marrow, then it is very likely that such integrin binding motifs combine to generate cell responses critical for the maintenance of the

mesenchymal cell niche. Thus, integrating a heterogeneous integrin binding approach into bioengineered substrates should be explored to achieve superior integrin stimulation on culture surfaces.

Our studies were focused on matrix integrins as the main signal mechanism that governs cell adhesion and survival on COL. Yet, other cell-substrate interactions triggered at the biomaterial interface may contribute to regulating cell growth and survival on HEP/COL substrates. For example, HEP not only acts as a growth factor reservoir but also serves co-receptor and co-factor functions,[26] which actively participate in matrix remodeling and cell survival. Heparin–collagen interactive functions extend beyond our in-vitro findings; this particular mixture of naturally derived materials has proven to be effective in promoting blood compatibility on thrombogenic COL matrixes by controlling clot formation,[66] tissue vascularization, and fibrin formation.[67] Overall, the body of evidence provided by HEP/COL substrates should be able to draw the attention of new researchers to develop novel and better COL-based materials not only for cell manufacturing but for tissue engineering.

Despite the benefits of using HEP/COL substrates for cell culture applications, their translation for scale-up systems in cell manufacture might be limited due to the xenogeneic source of individual components. Heparin and collagen 1 are both commercially available clinical products,[68,69] yet their xenogeneic derivation generates warnings to the FDA when intended for human somatic cell-based IND applications.[70] Whereas HEP can be replaced by other equivalent GAGs derived from recombinant sources,[71,72] collagen type I is primarily derived from bovine tendon and rat tail sources. Therefore, future commercial needs will require a scale-up translation to substrates employing COL motifs and recombinant GAGs to minimize health risks associated with xenogeneic components.

5 | CONCLUSION

In these studies, we performed a series of evaluations to identify a possible mechanism involved in the enhanced cell growth and potency reported by surface-deposited HEP/COL bilayers. Our findings implicate the COL integrin, $\alpha 2\beta 1$, in stimulating cell growth, survival, and immunomodulatory potency via the FAK-ERK½ mechanism. Moreover, HEP was shown to favor integrin-matrix signaling by supporting enhanced COL deposition on cultures, thus indirectly contributing to the FAK-ERK½ signaling cascade and downstream responses. Such findings were not observed on standard plastic and COL-coated surfaces, highlighting the value of multicomponent substrates in overcoming major challenges associated with decreased cell survival, yields, and potency in MSC cultures.

ACKNOWLEDGMENTS

We want to thank Integra Lifesciences Holdings Corporation in Añasco PR for contributing lyophilized collagen to our study and Ephraim Vazquez for assisting WB evaluations during the COVID-19 pandemic lockdown. The research reported in this publication was supported by the NSF-ERC for Cell Manufacturing Technologies No. EEC-1648035.

CONFLICT OF INTEREST STATEMENT

The authors declare no conflict of interest in this work.

DATA AVAILABILITY STATEMENT

The data that support the findings of this study are available from the corresponding author upon reasonable request.

ORCID

Said J. Cifuentes https://orcid.org/0000-0002-3674-8382
Maribella Domenech https://orcid.org/0000-0001-7061-8090

REFERENCES

1. Li H, Shen S, Fu H, et al. Immunomodulatory functions of mesenchymal stem cells in tissue engineering. *Stem Cells Int*. 2019;2019:9671206.
2. Spees JL, Lee RH, Gregory CA. Mechanisms of mesenchymal stem/stromal cell function. *Stem Cell Res Ther*. 2016;7:125.
3. Tozetti PA, Caruso SR, Mizukami A, et al. Expansion strategies for human mesenchymal stromal cells culture under xeno-free conditions. *Biotechnol Prog*. 2017;33:1358-1367.
4. Martin C, Olmos E, Collignon ML, et al. Revisiting MSC expansion from critical quality attributes to critical culture process parameters. *Process Biochem*. 2017;59:231-243.
5. Yuan X, Logan TM, Ma T. Metabolism in human mesenchymal stromal cells: a missing link between hMSC biomanufacturing and therapy? *Front Immunol*. 2019;10:977.
6. von Bahr L, Sundberg B, Lönnies L, et al. Long-term complications, immunologic effects, and role of passage for outcome in mesenchymal stromal cell therapy. *Biol Blood Marrow Transplant*. 2012;18:557-564.
7. Ho SS, Murphy KC, Binder BYK, Vissers CB, Leach JK. Increased survival and function of mesenchymal stem cell spheroids entrapped in instructive alginate hydrogels. *Stem Cells Transl Med*. 2016;5:773-781.
8. Ogle ME, Doron G, Levy MJ, Temenoff JS. Hydrogel culture surface stiffness modulates mesenchymal stromal cell secretome and alters senescence. *Tissue Eng Part A*. 2020;26:1259-1271.
9. Choi MR, Kim HY, Park JY, et al. Selection of optimal passage of bone marrow-derived mesenchymal stem cells for stem cell therapy in patients with amyotrophic lateral sclerosis. *Neurosci Lett*. 2010;472:94-98.
10. Kwee BJ, Sung KE. Engineering microenvironments for manufacturing therapeutic cells. *Exp Biol Med*. 2021;246:1845-1856.
11. Martino MM, Mochizuki M, Rothenfluh DA, Rempel SA, Hubbell JA, Barker TH. Controlling integrin specificity and stem cell differentiation in 2D and 3D environments through regulation of fibronectin domain stability. *Biomaterials*. 2009;30:1089-1097.
12. Lee JW, Juliano R. Mitogenic signal transduction by integrin- and growth factor receptor-mediated pathways. *Mol Cells*. 2004;17:188-202.
13. Illario M, Amideo V, Casamassima A, et al. Integrin-dependent cell growth and survival are mediated by different signals in thyroid cells. *J Clin Endocrinol Metab*. 2003;88:260-269.
14. Yen CF, Wang HS, Lee CL, Liao SK. Roles of integrin-linked kinase in cell signaling and its perspectives as a therapeutic target. *Gynecol Minim Invasive Ther*. 2014;3:67-72.
15. Filipenko NR, Attwell S, Roskelley C, Dedhar S. Integrin-linked kinase activity regulates Rac- and Cdc42-mediated actin cytoskeleton reorganization via alpha-PIX. *Oncogene*. 2005;24:5837-5849.
16. Huttenlocher A, Horwitz AR. Integrins in cell migration. *Cold Spring Harb Perspect Biol*. 2011;3:a005074.
17. Hastings JF, Skhinas JN, Fey D, Croucher DR, Cox TR. The extracellular matrix as a key regulator of intracellular signalling networks. *Br J Pharmacol*. 2019;176:82-92.

18. Reyes-Ramos AM, Álvarez-García YR, Solodin N, et al. Collagen I fibrous substrates modulate the proliferation and secretome of estrogen receptor-positive breast tumor cells in a hormone-restricted microenvironment. *ACS Biomater Sci Eng*. 2021;7:2430-2443.
19. Priya S, Sudhakaran PR. Cell survival, activation and apoptosis of hepatic stellate cells: modulation by extracellular matrix proteins. *Hepatol Res*. 2008;38:1221-1232.
20. Popov C, Radic T, Haasters F, et al. Integrins α2β1 and α11β1 regulate the survival of mesenchymal stem cells on collagen I. *Cell Death Dis*. 2011;2:e186.
21. Cifuentes SJ, Priyadarshani P, Castilla-Casadiego DA, Mortensen LJ, Almodóvar J, Domenech M. Heparin/collagen surface coatings modulate the growth, secretome, and morphology of human mesenchymal stromal cell response to interferon-gamma. *J Biomed Mater Res A*. 2021;109:951-965.
22. Haseli M, Castilla-Casadiego DA, Pinzon-Herrera L, et al. Immunomodulatory functions of human mesenchymal stromal cells are enhanced when cultured on HEP/COL multilayers supplemented with interferon-gamma. *Mater Today Bio*. 2022;13:100194.
23. Pinzon-Herrera L, Mendez-Vega J, Mulero-Russe A, Castilla-Casadiego DA, Almodovar J. Real-time monitoring of human Schwann cells on heparin-collagen coatings reveals enhanced adhesion and growth factor response. *J Mater Chem B Mater Biol Med*. 2020;8:8809-8819.
24. Takada Y, Ye X, Simon S. The integrins. *Genome Biol*. 2007;8:215.
25. Benoit DSW, Anseth KS. Heparin functionalized PEG gels that modulate protein adsorption for hMSC adhesion and differentiation. *Acta Biomater*. 2005;1:461-470.
26. Hill KE, Lovett BM, Schwarzbauer JE. Heparan sulfate is necessary for the early formation of nascent fibronectin and collagen I fibrils at matrix assembly sites. *J Biol Chem*. 2022;298:101479.
27. Sobel M, Fish WR, Toma N, et al. Heparin modulates integrin function in human platelets. *J Vasc Surg*. 2001;33:587-594.
28. Da Silva MS, Horton JA, Wijelath JM, et al. Heparin modulates integrin-mediated cellular adhesion: specificity of interactions with alpha and beta integrin subunits. *Cell Commun Adhes*. 2003;10:59-67.
29. Castilla-Casadiego DA, Pinzon-Herrera L, Perez-Perez M, Quiñones-Colón BA, Suleiman D, Almodovar J. Simultaneous characterization of physical, chemical, and thermal properties of polymeric multilayers using infrared spectroscopic ellipsometry. *Colloids Surf A Physicochem Eng Asp*. 2018;553:155-168.
30. Christy BA, Herzig MC, Delavan CP, et al. Use of multiple potency assays to evaluate human mesenchymal stromal cells. *J Trauma Acute Care Surg*. 2020;89:S109-S117.
31. Decher GHJD, Hong JD, Schmitt J. Buildup of ultrathin multilayer films by a self-assembly process: III. Consecutively alternating adsorption of anionic and cationic polyelectrolytes on charged surfaces. *Thin Solid Films*. 1992;210–211:831-835.
32. Nunes AM, Minetti CASA, Remeta DP, Baum J. Magnesium activates microsecond dynamics to regulate integrin-collagen recognition. *Structure*. 2018;26:1080-1090.e5.
33. Davidenko N, Schuster CF, Bax DV, et al. Evaluation of cell binding to collagen and gelatin: a study of the effect of 2D and 3D architecture and surface chemistry. *J Mater Sci Mater Med*. 2016;27:148.
34. Salemi Z, Azizi R, Fallahian F, Aghaei M. Integrin α2β1 inhibition attenuates prostate cancer cell proliferation by cell cycle arrest, promoting apoptosis and reducing epithelial-mesenchymal transition. *J Cell Physiol*. 2021;236:4954-4965.
35. Cheng T-M, Chang WJ, Chu HY, et al. Nano-strategies targeting the integrin αvβ3 network for cancer therapy. *Cell*. 2021;10:1684.
36. Barczyk M, Carracedo S, Gullberg D. Integrins. *Cell Tissue Res*. 2010;339:269-280.
37. Kapp TG, Rechenmacher F, Neubauer S, et al. A comprehensive evaluation of the activity and selectivity profile of ligands for RGD-binding integrins. *Sci Rep*. 2017;7:39805.
38. Elango J, Hou C, Bao B, Wang S, Maté Sánchez de Val JE, Wenhui W. The molecular interaction of collagen with cell receptors for biological function. *Polymers*. 2022;14:14.
39. San Antonio JD, Lander AD, Karnovsky MJ, Slayter HS. Mapping the heparin-binding sites on type I collagen monomers and fibrils. *J Cell Biol*. 1994;125:1179-1188.
40. Xv J, Ming Q, Wang X, et al. Mesenchymal stem cells moderate immune response of type 1 diabetes. *Cell Tissue Res*. 2017;368:239-248.
41. Fang D, Chen B, Lescoat A, Khanna D, Mu R. Immune cell dysregulation as a mediator of fibrosis in systemic sclerosis. *Nat Rev Rheumatol*. 2022;18:683-693.
42. McClain-Caldwell I, Vitale-Cross L, Mayer B, et al. Immunogenic potential of human bone marrow mesenchymal stromal cells is enhanced by hyperthermia. *Cytotherapy*. 2018;20:1437-1444.
43. Jin L, Deng Z, Zhang J, et al. Mesenchymal stem cells promote type 2 macrophage polarization to ameliorate the myocardial injury caused by diabetic cardiomyopathy. *J Transl Med*. 2019;17:251.
44. Wu C, Xue Y, Wang P, et al. IFN-γ primes macrophage activation by increasing phosphatase and tensin homolog via downregulation of miR-3473b. *J Immunol*. 2014;193:3036-3044.
45. Curtsinger JM, Agarwal P, Lins DC, Mescher MF. Autocrine IFN-γ promotes naive CD8 T cell differentiation and synergizes with IFN-α to stimulate strong function. *J Immunol*. 2012;189:659-668.
46. Mihara M, Hashizume M, Yoshida H, Suzuki M, Shiina M. IL-6/IL-6 receptor system and its role in physiological and pathological conditions. *Clin Sci*. 2012;122:143-159.
47. Scheller J, Chalaris A, Schmidt-Arras D, Rose-John S. The pro- and anti-inflammatory properties of the cytokine interleukin-6. *Biochim Biophys Acta – Mol Cell Res*. 2011;1813:878-888.
48. Fremd C, Schuetz F, Sohn C, Beckhove P, Domschke C. B cell-regulated immune responses in tumor models and cancer patients. *Onco Targets Ther*. 2013;2:e25443.
49. Khan IA, MacLean JA, Lee FS, et al. IP-10 is critical for effector T cell trafficking and host survival in toxoplasma gondii infection. *Immunity*. 2000;12:483-494.
50. Beutler B, Cerami A. The biology of Cachectin/TNF – a primary mediator of the host response. *Annu Rev Immunol*. 1989;7:625-655.
51. Yadav A, Saini V, Arora S. MCP-1: chemoattractant with a role beyond immunity: a review. *Clin Chim Acta*. 2010;411:1570-1579.
52. Bethel-Brown C, Yao H, Hu G, Buch S. Platelet-derived growth factor (PDGF)-BB-mediated induction of monocyte chemoattractant protein 1 in human astrocytes: implications for HIV-associated neuroinflammation. *J Neuroinflammation*. 2012;9:262.
53. Mukaida N. Interleukin-8: an expanding universe beyond neutrophil chemotaxis and activation. *Int J Hematol*. 2000;72:391-398.
54. Rao VV, Vu MK, Ma H, Killaars AR, Anseth KS. Rescuing mesenchymal stem cell regenerative properties on hydrogel substrates post serial expansion. *Bioeng Transl Med*. 2019;4:51-60.
55. Chen X-D. Extracellular matrix provides an optimal niche for the maintenance and propagation of mesenchymal stem cells. *Birth Defects Res C Embryo Today*. 2010;90:45-54.
56. Peysselon F, Ricard-Blum S. Heparin–protein interactions: from affinity and kinetics to biological roles. Application to an interaction network regulating angiogenesis. *Matrix Biol*. 2014;35:73-81.
57. Sakiyama-Elbert SE, Hubbell JA. Development of fibrin derivatives for controlled release of heparin-binding growth factors. *JCR*. 2000;65:389-402.
58. Rabenstein DL. Heparin and heparan sulfate: structure and function. *Nat Prod Rep*. 2002;19:312-331.
59. Schönherr E, Hausser HJ. Extracellular matrix and cytokines: a functional unit. *Dev Immunol*. 2000;7:89-101.
60. Ejaz U, Akhtar F, Xue J, Wan X, Zhang T, He S. Review: inhibitory potential of low molecular weight heparin in cell adhesion; emphasis on tumor metastasis. *Eur J Pharmacol*. 2021;892:173778.

61. Xu X, Dai Y. Heparin: an intervenor in cell communication. *J Cell Mol Med*. 2010;14:175-180.
62. Castilla-Casadiego DA, García JR, García AJ, Almodovar J. Heparin/-collagen coatings improve human mesenchymal stromal cell response to interferon gamma. *ACS Biomater Sci Eng*. 2019;5:2793-2803.
63. Clark AY, Martin KE, García JR, et al. Integrin-specific hydrogels modulate transplanted human bone marrow-derived mesenchymal stem cell survival, engraftment, and reparative activities. *Nat Commun*. 2020;11:114.
64. Malcor J-D, Mallein-Gerin F. Biomaterial functionalization with triple-helical peptides for tissue engineering. *Acta Biomater*. 2022;148:1-2.
65. Munnix ICA, Gilio K, Siljander PR, et al. Collagen-mimetic peptides mediate flow-dependent thrombus formation by high- or low-affinity binding of integrin alpha2beta1 and glycoprotein VI. *J Thromb Haemost*. 2008;6:2132-2142.
66. Ascherl R, Blümel G, Stemberger A. Kollagen, ein Biomaterial in der Medizin. *Hamostaseologie*. 1990;10:164-176.
67. van Wachem PB, Plantinga JA, Wissink MJB, et al. In vivo biocompatibility of carbodiimide-crosslinked collagen matrices: effects of cross-link density, heparin immobilization, and bFGF loading. *J Biomed Mater Res*. 2001;55:368-378.
68. Avila Rodríguez MI, Rodríguez Barroso LG, Sánchez ML. Collagen: a review on its sources and potential cosmetic applications. *J Cosmet Dermatol*. 2018;17:20-26.
69. Onishi A, St Ange K, Dordick JS, Linhardt R. Heparin and anticoagulation. *J Front Biosci*. 2016;21:1372-1392.
70. US Food and Drug Administration. *Guidance for FDA Reviewers and Sponsors: Content and Review of Chemistry, Manufacturing, and Control (CMC) Information for Human Somatic Cell Therapy Investigational New Drug Applications (INDs)*. CBER; 2008.
71. Farrugia BL, Lord MS, Melrose J, Whitelock JM. Can we produce heparin/heparan sulfate biomimetics using 'mother-nature' as the gold standard? *Molecules*. 2015;20:4254-4276.
72. Lord MS, Cheng B, Tang F, Lyons JG, Rnjak-Kovacina J, Whitelock JM. Bioengineered human heparin with anticoagulant activity. *Metab Eng*. 2016;38:105-114.

SUPPORTING INFORMATION

Additional supporting information can be found online in the Supporting Information section at the end of this article.

How to cite this article: Cifuentes SJ, Domenech M. Heparin–collagen I bilayers stimulate FAK/ERK½ signaling via α2β1 integrin to support the growth and anti-inflammatory potency of mesenchymal stromal cells. *J Biomed Mater Res*. 2024; 112(1):65-81. doi:10.1002/jbm.a.37614